

An iterative Bayesian approach for nearly automatic liver segmentation: algorithm and validation

M. Freiman · O. Eliassaf · Y. Taieb · L. Joskowicz ·
Y. Azraq · J. Sosna

Received: 7 January 2008 / Accepted: 18 June 2008
© CARS 2008

Abstract

Purpose We present a new algorithm for nearly automatic liver segmentation and volume estimation from abdominal Computed Tomography Angiography (CTA) images and its validation.

Materials and methods Our hybrid algorithm uses a multiresolution iterative scheme. It starts from a single user-defined pixel seed inside the liver, and repeatedly applies smoothed Bayesian classification to identify the liver and other organs, followed by adaptive morphological operations and active contours refinement. We evaluate the algorithm with two retrospective studies on 56 validated CTA images. The first study compares it to ground-truth manual segmentation and semi-automatic and automatic commercial methods. The second study uses the public data-set SLIVER07 and its comparison methodology.

Results We achieved for both studies, correlations of 0.98 and 0.99 for liver volume estimation, with mean volume differences of 5.36 and 2.68% with respect to manual ground-truth estimation, and mean volume variability for different initial seeds of 0.54 and 0.004%, respectively. For the second study, our algorithm scored 71.8 and 67.87 for the training and test datasets, which compares very favorably with other semi-automatic methods.

Conclusions Our algorithm requires minimal interaction by a non-expert user, is accurate, efficient, and robust to initial

seed selection. It can be effective for hepatic volume estimation and liver modeling in a clinical setup.

Keywords Computed tomography · Segmentation of abdominal organs · Computer-assisted diagnosis

Introduction

Liver segmentation and volume estimation from abdominal computed tomography angiography (CTA) images is a key task in many clinical applications. It includes the assessment of hepatomegaly and liver cirrhosis, liver regeneration after hepatectomy, hepatic transplantation planning for size compatibility, and monitoring of patients with liver metastases, where the disease is related to an enlargement of the liver, among others. To be of practical clinical use, the liver segmentation and liver volume estimation must be accurate, fast, robust, and nearly automatic, so that radiologists can perform it without the help of a technician.

Nearly automatic liver segmentation, which is essential for hepatic volumetry, is known to be a very challenging task due to the ambiguity of liver boundaries, the complexity of the liver surface, and the presence of surrounding organs. Many previous works propose automatic or semi-automatic methods for liver segmentation. These methods can be classified into four main categories: (1) atlas-guided methods [1–3]; (2) region growing methods [4,5]; (3) deformable models and level sets based methods [6,7], and; (4) classification based methods [8,9]. In many cases, the methods produce inaccurate segmentations, as they do not make full use of the intensity and geometric information present in the original images.

To circumvent this problem, a hybrid two-phase approach consisting of a preliminary segmentation (usually atlas- or

M. Freiman (✉) · O. Eliassaf · Y. Taieb · L. Joskowicz
School of Engineering and Computer Science,
The Hebrew University of Jerusalem,
Givat Ram Campus, Jerusalem 91904, Israel
e-mail: freiman@cs.huji.ac.il

Y. Azraq · J. Sosna
Department of Radiology, School of Medicine,
Hadassah Hebrew University Medical Center, Jerusalem, Israel

intensity-based) followed by a deformable model refinement was proposed [10, 11]. This approach works well when the preliminary segmentation is close to the final one, since if it is off (e.g., due to a local minima), it is very unlikely that the refinement step will manage to significantly improve it.

Metaxas et al. [12] propose a hybrid iterative scheme for general object segmentation. In this scheme, the results of one method are used by the second one repeatedly until convergence. Specifically, this method computes first a Markov random field from manually selected initial pixel seeds inside each organ, and then uses it as the initial mesh for deformable model based segmentation. The process is repeated with the resulting contour until convergence. The advantage of this method is that while each iteration produces only small modifications, the accumulated modification can be significant. However, the computation of 3D Markov Random Fields is computationally expensive, so the implementation uses 2D fields instead, with the consequent sacrifice in accuracy.

The disadvantages of the semi-automatic methods [4–7, 12] are that most of them require significant user interaction, such as the selection of multiple pixel seeds, or the manual drawing of initial contours. This initialization is time-consuming and user-dependent, which significantly affects the robustness of the methods. Because of the liver boundary ambiguity, expert radiological knowledge, which is not always available, is often required to obtain a proper initialization. Automatic methods [1–3] do not require user initialization but depend on good prior shape models, which are sensitive to shape variations between healthy and sick livers, different patient ages, and image scanning protocols.

In this paper, we present a hybrid, nearly automatic liver segmentation algorithm that uses an iterative classification scheme. The algorithm repeatedly applies multiresolution smoothed Bayesian classification followed by adaptive morphological operations and active contours refinement. The smoothed Bayesian classification uses patient-specific ‘soft’ thresholding coupled with neighborhood information instead of a simple binary threshold [10, 11] for a more accurate classification. Adjacent organs and tissues are explicitly removed during the classification step using an intensity distribution model developed for this purpose. The resulting segmentation is refined with an active contours step.

To evaluate and validate our algorithm accuracy and robustness, we performed two retrospective studies on validated clinical datasets totaling 56 CTA images. In the first study, which consists of 26 CTA scans, we compared the results of our algorithm to those of a ground-truth manual segmentation and semi-automatic and automatic commercial methods. The evaluation includes both the volume and surface measurements. In the second study, we used the SLIVER07 (Segmentation of the Liver Competition 2007) dataset, a publicly available database of 30 CTA images [18]. We compared the results to their ground-truth segmentation

and other published methods. In both the studies, the proposed algorithm achieved a high score among semi-automatic methods with much less user interaction and lower variability.

Method

Our algorithm consists of three main steps: (1) intensity-based classification; (2) adaptive morphological adjustment, and; (3) geodesic active contours refinement. After each iteration, the internal parameters of the classification step are updated before its application. This coupling is designed to overcome a biased classification due to ambiguous liver boundaries and biased pixel seed selection. To speed up the segmentation and make it more robust and accurate, the algorithm uses a multiresolution approach. Starting from the coarsest level of the image pyramid, the algorithm iterates on each level until convergence, and then switches to the next, more refined level. The final step is performed at full resolution on the original image. Table 1 outlines the procedure. We describe each step in detail next.

Intensity-based classification

Intensity model generation

The first step of the algorithm is the construction of an intensity model that differentiates between the liver and other organs and tissues, which are interpreted as background. The main challenges are to handle the ambiguous boundary between the liver and other organs, such as the kidney, and to properly identify the background organs. To overcome these difficulties, we propose to use a five-class model for voxel classification according to their gray level value.

The first class represents the liver. The remaining four classes represent other organs and tissues whose gray level

Table 1 Outline of the liver segmentation algorithm

Input: voxel seed inside the liver, selected manually.

1. Intensity-based classification

1. Intensity model generation
2. Voxel classification with smoothed MAP rule

2. Adaptive morphological operations

1. Largest connected component selection
2. Hole filling
3. Morphological opening

3. Geodesic active contours refinement

1. Energy image generation
2. Active contours refinement

Repeat 1–3 until convergence.

Output: Liver contour segmentation and voxel classification.

values are above or below the liver class. We model each class with a normal distribution defined by its intensity mean and variance values. In the first iteration, the mean and the variance of a rectangular neighborhood around the user-selected pixel seed inside the liver are computed and taken as the initial parameter values of the liver class.

In subsequent iterations, the segmented region from the previous iteration is used to compute the mean and variance values of the liver class. The remaining four classes model organs near and far (above/below) the liver in the intensity domain. The mean value of each class is computed with respect to the liver class mean value. Formally, the liver class X_{liver} is defined as:

$$X_{liver} \sim N(\mu_{liver}, \sigma_{liver}^2) \tag{1}$$

The other four classes X_i are modeled as:

$$X_i \sim N(\mu_i, \sigma_i^2) \tag{2}$$

for each $i \in \{near-low, near-high, far-low, far-high\}$. The means of these classes are defined as:

$$\begin{aligned} \mu_{near-high} &= \mu_{liver} + (k_{near} \times \sigma_{liver}) \\ \mu_{near-low} &= \mu_{liver} - (k_{near} \times \sigma_{liver}) \\ \mu_{far-high} &= \mu_{liver} + (k_{far} \times \sigma_{liver}) \\ \mu_{far-low} &= \mu_{liver} - (k_{far} \times \sigma_{liver}) \end{aligned} \tag{3}$$

where the factors k_{near} and k_{far} are determined from Chebyshev's inequality:

$$Pr(|X_i - \mu_{liver}| \geq k\sigma_{liver}) \leq \frac{1}{k^2} \tag{4}$$

This inequality ensures that at least $(1 - \frac{1}{k^2}) \times 100\%$ of the values are within k standard deviations from the mean value. This ensures that each voxel from the ambiguous liver boundary has a high probability of being in both the liver and near classes. Its final classification will then depend on its neighboring voxels. Initially, we set $\sigma_i = \sigma_{liver}$ for all classes.

The values of the parameters k_{near} and k_{far} are set experimentally by searching the two-dimensional parameter space in the appropriate parameter intervals. Each vector of the parameter values is ranked by comparing the segmentation results using these parameter values on the training datasets to their ground truth segmentation. Figure 1 shows an example plot of the liver distributions and its two nearby classes.

Voxel classification

The second step is the unique classification of each voxel. The classification relies on the voxels intensity values and their neighboring voxels. Neighborhood information is important since voxel intensity values are correlated. Our classification follows the three-step method by Teo et al. [13] (Table 2).

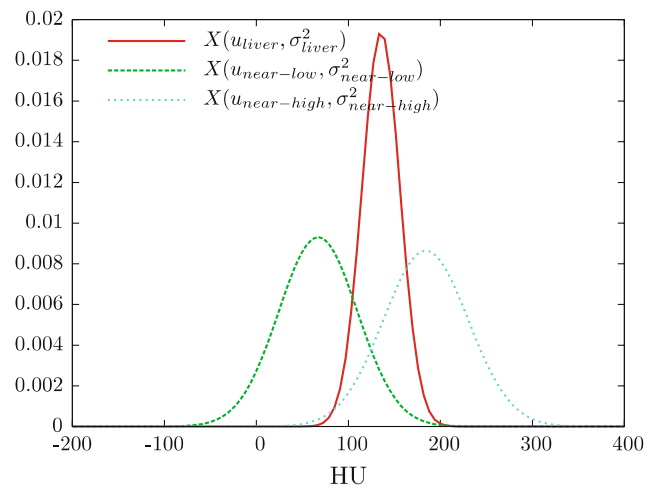


Fig. 1 The estimated Gaussian distributions of the liver and its two nearby classes as computed by our method. The horizontal axis are gray level Hounsfield units, while the vertical axis are class probabilities

Table 2 Voxel classification with a smoothed MAP rule

<p>Input: An intensity model described with classes</p> <ol style="list-style-type: none"> 1. Generate for each class a membership map from the volume based on the class intensity model 2. Smooth the membership maps using an anisotropic diffusion process 3. Compute the segmentation label map with the maximum posterior (MAP) rule <p>Output: Segmentation label map</p>

In the first step, we compute the probability $C_{(j,i)}$ of a voxel V_j with intensity value v_j to belong to class c_i , where $i \in \{liver, near-low, near-high, far-low, far-high\}$ using Bayes rule:

$$Pr(v_j|c_i) \propto Pr(c_i|v_j)Pr(c_i) \tag{5}$$

where $Pr(c_i|v_j)$ is obtained from the intensity model generated in the previous step, and $Pr(c_i)$ is assumed to be from a uniform distribution. The resulting five maps quantify the membership probability of each voxel to each class.

Next, we incorporate the neighborhood information to the classification process by smoothing the probability maps $C_{(j,i)}$ for each class i separately using the anisotropic diffusion equation proposed by Perona and Malik [14]:

$$\frac{\partial I}{\partial t} = \nabla \cdot a \nabla I, \quad \text{with } a = e^{-\frac{|\nabla I|^2}{b^2}} \tag{6}$$

where ∇I is the image gradient, and a is the conductivity coefficient of the local image edges smoothing, which inversely depends on the image gradient magnitude and scaling factor b that helps to differentiate between noise and real image gradients. The anisotropic smoothing process flattens small peaks in the membership probability maps, most likely

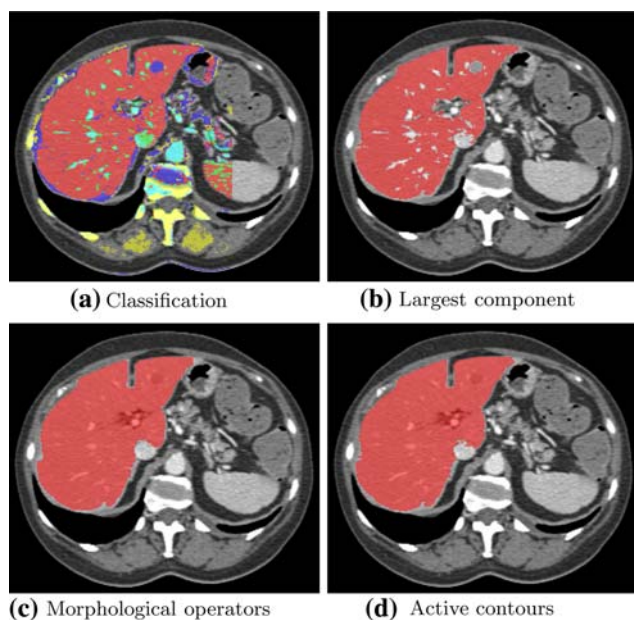


Fig. 2 Illustration of the segmentation steps: **a** Smoothed Bayesian classification. **b** Largest connected component selection. **c** Application of morphological operators. **d** Active contours refinement

misclassification, while preserving sharp edges between different objects.

Finally, we apply the maximum posterior (MAP) rule:

$$C_{(j,\text{final})} = \underset{c_i}{\operatorname{argmax}} Pr(v_j|c_i) \quad (7)$$

The rule sets the final membership of each voxel to the class with the highest probability. The binary segmentation image is generated by selecting only the voxels that belong to the liver class. Figure 2a shows an example of a classified slice.

Adaptive morphological adjustment

The third step is the identification of the liver region. The previous classification yields most of the liver region, additional disconnected regions outside the liver, and holes inside the liver. Regions outside the liver correspond to anatomical structures with intensity values similar to that of the liver, such as the kidney and the spleen. Holes correspond to small tumors and artery and portal veins inside the liver whose intensity values are distinctly different from the liver intensity values due to the use of the imaging contrast agent. To obtain the correct liver segmentation, the disconnected regions must be eliminated, and the holes inside the liver must be filled. This is done with a set of adaptive morphological operators.

We first remove the disconnected regions outside the liver by identifying the largest connected component in the labeled image, as illustrated in Fig. 2b. Next, we use a closing morphological operator to fill holes inside the liver, followed by an opening operator to separate the liver from surroun-

ding organs such as the kidney, the spleen, and the heart. The operators radiuses are adaptively computed from the liver volume estimation V_{liver} obtained from the previous classification step with:

$$\begin{aligned} R_{\text{open}} &= V_{\text{liver}} * C \\ R_{\text{close}} &= R_{\text{open}} * R \end{aligned} \quad (8)$$

where C and R are predefined radius constants computed by searching the two-dimensional parameter space in the appropriate parameter intervals. The adaptive parameter adjustment of the morphological operators allows the accurate and automatic application of the morphological operators to achieve the required liver segmentation. The result of this step is an updated labeled map of the liver, as illustrated in Fig. 2c.

Geodesic active contours refinement

The classification and the morphological adjustment may miss parts of the liver volume. In addition, the liver boundaries may be inaccurate in several regions. To correct this, we repeatedly apply a fine-tuning active contours segmentation [15]:

$$F = \alpha g_I + \beta c g_I + \gamma (\nabla g_I \cdot \mathbf{N}) \quad (9)$$

where g_I is the speed function derived from the gradient magnitude of the input image I , c is the mean curvature of the contour, \mathbf{N} is the normal of the voxel, and α , β , and γ are weights that modulate the relative contributions of the three components of F . This equation is solved using the level-set method, where the deformed contour is represented as the zeroth level set of the function ϕ :

$$\frac{\partial}{\partial t} \phi(x, t) = F \nabla \phi \quad (10)$$

defined at every voxel in the input image, where x is the voxel coordinate and t is the time point.

Since the active contours method is well suited for structures bounded by strong image intensity edges, we emphasize the liver boundaries by applying a windowing function to the original image:

$$I'(x) = \begin{cases} \mu_{\text{liver}} + \sigma_{\text{liver}} & \text{if } I(x) > \mu_{\text{liver}} + \sigma_{\text{liver}}, \\ I(x) & \text{if } \mu_{\text{liver}} - \sigma_{\text{liver}} \leq I(x) \\ & \text{or } I(x) \leq \mu_{\text{liver}} + \sigma_{\text{liver}}, \\ \mu_{\text{liver}} - \sigma_{\text{liver}} & \text{if } I(x) < \mu_{\text{liver}} - \sigma_{\text{liver}}. \end{cases} \quad (11)$$

where I' is the new image, I is the original image, and μ_{liver} and σ_{liver} are the liver class parameters as computed in the intensity model step. Figure 2d illustrates the result of this step.

Algorithm iterations

The intensity based classification, morphological operators, and active contours steps are repeatedly applied to the image until no further change occurs (Table 1). The iterations are necessary for fine-tuning the intensity model to improve the classification and minimize the importance of the initial voxel seed selection. The intensity based classification updates the classes model by computing the mean and variance of the liver class from the current liver region and updating the other four classes by computing their mean and variance parameters with Eq. 3. The morphological operations are then applied on the resulting classes to find the new liver region. The active contours refinement improves the liver boundaries fitting.

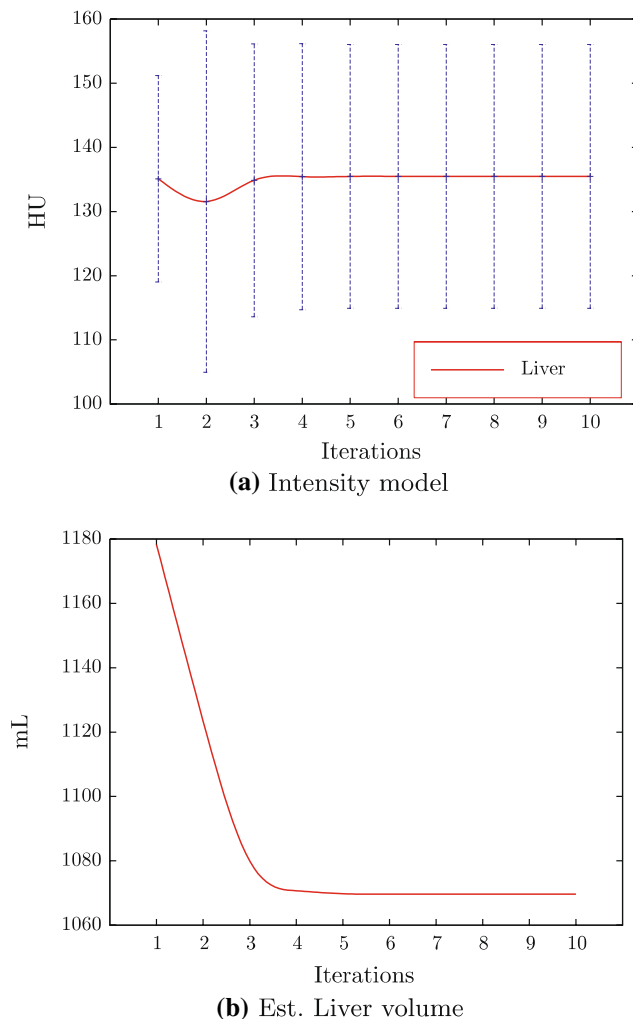


Fig. 3 Updates during the iterative scheme. **a** Intensity model (mean and standard deviation of liver). The horizontal axis represents the number of iterations; the vertical axis represents the mean (point) and variance (interval) of the liver class in Hounsfield units (HU). **b** Estimated liver volume (in ml) during the iterations

The algorithm starts on a coarse level of the image pyramid. The switching criterion between pyramid levels is convergence at a given resolution level. Starting from the coarsest level of the pyramid, the algorithm iterates on each level until convergence, and then switches to the next more refined level on the pyramid. The final step is performed on the original image, at full resolution.

Figure 3 illustrates the importance of the iterations in the fine-tuning of the liver intensity model and in the corresponding liver volume estimation. Figure 3a shows the liver class parameters according to the algorithm iterations. In the first iteration, the parameters were computed according to the manually selected pixel seed. In the remaining iterations, the mean and variance of the liver class were updated according to the segmented liver region. Note the significant change in the estimated variance during the iterations. Figure 3b shows the changes in the estimated liver volume during the iterative process. Note how the estimated liver volume converges to its final estimation in several iterations.

Experimental validation

To evaluate our algorithm, we implemented it with ITK software library [16] and with the smoothed Bayesian classification module from [17]. We conducted two retrospective studies on two validated clinical datasets totaling 56 CTA scans. Figure 4 illustrates the result of our algorithm on one of the datasets.

Parameter setup

The algorithm internal parameter values were empirically set after exploration on 10 CTA test images as follows. The classification parameters in Eq. 3 were set to $k_{\text{near}} = 2.2$ and $k_{\text{far}} = 4$. These parameter values guarantee by Chebyshev's inequality Eq. 4 that at least 80% of the liver voxels are classified as liver, and at least 70% of the voxels that belong to the near classes will be classified as near, even if the normal distribution of the liver intensities assumption is not correct. The morphological operation parameters in Eq. 8 were set to $C = 4$ and $R = 1.2$. Note that the values are in millimeters, not voxels, to properly model the anisotropic nature of the data. Each pair of parameters was determined after about 20 runs on the test CTA images. Each pair of parameter values was ranked by comparing the segmentation results using the predetermined parameter values on the training dataset to their ground truth segmentation. The values of the highest ranking pair were then selected. The parameters of the geodesic active contours (Eq. 9) module were set as follows: the propagation parameter was set to $\alpha = -1$, the curvature scaling term and the advection term were set

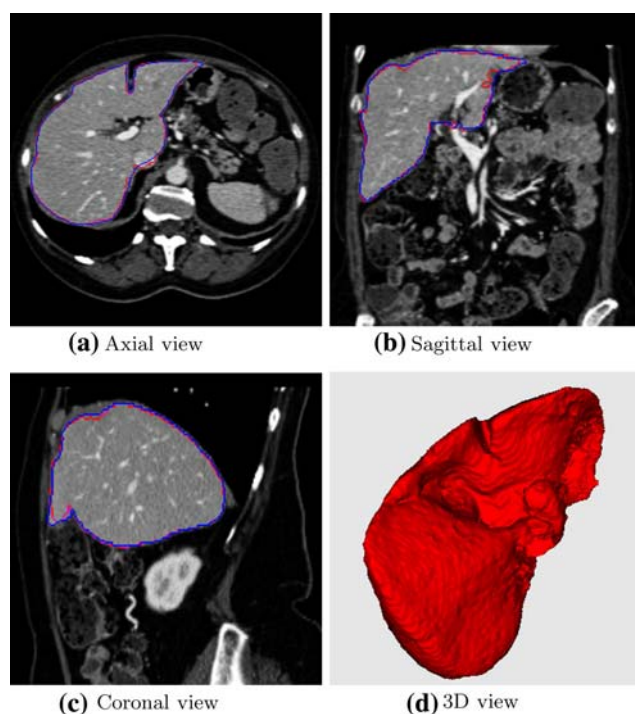


Fig. 4 Example of a segmented liver. The *red contour* is our segmentation result, and the *blue contour* is the ground-truth segmentation. For 3D movies that illustrate the algorithm results, please refer to: <http://www.cs.huji.ac.il/~freiman/LiverSeg>

both to $c = \gamma = 0.33$. The number of iterations of the active contours step was set to 7 for each iteration of the algorithm.

We used a three-level multiresolution pyramid precomputed from the original CTA images. The anisotropic smoothing parameters of the classification probability maps in Eq. 6 were set to $b = 1$ for the conductance term and to $t = 0.0625$ for the time-step. The smoothing process performs two iterations at the coarsest level of the image pyramid and four iterations in the two subsequent levels.

First study

The first study compares our algorithm to ground-truth manual segmentation and to semi-automatic and automatic commercial methods.

The study dataset consists of 26 CT scans from 26 adult patients (average age 54 years; range 32–78). The scans were acquired in a 16-channel detector scanner (Brilliance 16, Philips Medical Systems, Groningen, The Netherlands) with 2mm slice thickness and 1mm increment (200–250 mAs, 120 kVp). The clinical findings of these scans included 13 healthy livers, 3 livers with cirrhosis, 4 with metastases, and 6 with primary liver tumors. The dataset was used in a previous study by Sosna et al. [9].

We compared the results of our method to those obtained from a manual tracing of the liver contour in each slice

performed by a dedicated technologist on a Vitrea 2 workstation (Vital Images, Plymouth, MN, USA), which serves as the ground-truth. In addition, we compared our method to a prototype automatic segmentation tool and a semi-automatic paint-brush tool in a Philips EBW 3.0 workstation, (Philips Medical Systems, Groningen, The Netherlands). The results of these methods were reported by Sosna et al. [9].

The liver scans were segmented with each method. The liver volume estimates were then computed directly from the resulting segmentation. The liver volumes were compared to the ground-truth using linear regression analysis. User interaction and computation times were also recorded. In addition, we evaluated the robustness of our algorithm and the commercial automatic method (2) by comparing the volume differences of three runs with different initialization seeds. Since we did not have access to the manual segmentation, we could not compare our segmentation to the gold standard using other measures, as we did in the second study.

The mean liver volume computed from the manual tracing was 1,657 mL (milliliters), with a range of 1,050–2,647 mL. The mean liver volume computed with our method (1) was 1,648 mL (range 981–2744 mL), with the commercial automatic method (2) 1479 mL (range 926–2,417 mL) and with the commercial semi-automatic method (3) 1,619 mL (range 1,018–2,541 mL). Our method estimated the liver volume much better than the commercial automatic algorithm.

Table 3 summarizes the other measurement results. The mean absolute difference between the estimated liver volumes between manual tracing and our method was 5.36% (std = 3.48%) of the liver volume, with the commercial automatic method it was 10.55% (std 5.98%), and with commercial semi-automatic method it was 2.65% (std = 1.45%). These results indicate that our algorithm estimated the liver volume more accurately than the commercial automatic method. The calculated correlation coefficient for liver volume between the manual tracing and our method measurements was 0.98, which is better than the correlation of the other methods. The correlation between the commercial automatic method and the ground-truth was 0.97, and

Table 3 First study experimental results summary for 26 CTA scans

Method	Volume diff. %	Corr. coeff.	Variations %
1. Ours	5.36 (3.48)	0.98	0.54 (0.76)
2. Commercial automatic	10.55 (5.98)	0.97	2.09 (2.85)
3. Commercial semi-automatic	2.65 (1.48)	0.99	–

The first column indicates the method used. The *second column* shows the estimated volume difference (mean and standard deviation in parenthesis). The third column shows the correlation coefficient with the ground-truth manual tracing segmentation. The last column shows the mean (std) volume estimation variations for the different seed selections

between the commercial semi-automatic method and the ground-truth was 0.99. The mean volume difference between initializations with different pixel seeds with our method was 0.54% (std = 0.76%) and 2.09% (std = 2.85%) with the commercial automatic method, which indicates that our algorithm is highly robust to seed selection.

The mean segmentation time of the manual tracing was 7:24 min, most of it was user time. Our method required a few seconds of user time for pixel seed selection and a mean of 23:22 min for processing on a standard PC. The commercial automatic method running time was 0:37 min on dedicated workstation, which is not directly comparable to our method running time. The commercial semi-automatic method total segmentation time was 5:14 min. Most of it was user time due to its interactive method.

Second study

For the second study, we used the SLIVER07 (Segmentation of the Liver Competition 2007) [18] publicly available database and comparison methodology. We compared the results to their ground-truth segmentation and other available methods.

The dataset consists of 30 CTA images with ground-truth manual segmentations validated by two experts. The dataset consists of two parts. The first 20 scans were used as a training set and include the ground-truth segmentations. The remaining 10 CTA scans were used as test sets, and their ground-truth segmentations are not accessible. Five measures were computed: (1) volumetric overlap error; (2) absolute volume difference; (3) average symmetric surface distance; (4) root mean squares (RMS) symmetric surface distance, and; (5) maximum symmetric surface distance. The measures and aggregate grade were computed on the test set by the database providers as described in [18].

Table 4 summarizes the results of our method. The average values for the test and training sets were as follows: (1) volumetric overlap error 8.55 and 7.81%; (2) absolute volume difference 2.78 and 2.63%; (3) average symmetric surface distance 1.46 and 1.28 mm; (4) root mean squares (RMS) symmetric surface distance 2.94 and 2.55 mm, and; (5) maxi-

Table 4 Second study experimental results summary for 30 CTA scans from the SLIVER07 datasets

Dataset	Volume diff. %	Corr. coeff	Variations %
1. Training	2.63 (1.64)	0.99	0.004 (0.005)
2. Test	2.78 (2.14)	–	–

The first column indicates the dataset. The second column shows the estimated mean (std) volume difference. The third column shows the correlation with the ground-truth manual tracing segmentation. The last column shows the mean (std) volume estimation variations for the different seed selections

imum symmetric surface distance 26.72 and 22.77 mm. The correlation between our volume estimation and the ground truth on the training set was 0.99. Note that since the ground-truth is not available for the test set, we could not compute the correlation value for it. Note also that this detailed quantitative evaluation was not possible for the first database, as no ground-truth segmentations were available to us.

We also evaluated the robustness of our method by repeatedly selecting different initial seeds and comparing the results. We chose three different seeds initializations on the training dataset of 20 CTA images. The absolute volume difference was 0.004%, which is negligible.

The results suggest that our method is both accurate and robust to pixel seed selection. Our method achieved a total score of 71.8 on the training set and of 67.87 on the test set as computed in [18]. It is ranked forth of the semi-automatic method. However, all other semi-automatic methods require significantly more user interaction and therefore, are more time-consuming and less robust to different user interactions.

Conclusions

We have presented a new algorithm for the nearly automatic liver segmentation and volume estimation from abdominal CTA images. The hybrid algorithm uses a multiresolution iterative scheme that comprises a smoothed Bayesian classification coupled with set of adaptive morphological operations and active contours refinement.

The main advantages of our method are that it requires minimal user interaction for initialization—a single pixel seed inside the liver—does not require any adjustment of the internal parameters, is robust, and can be performed by non-experts. The multiresolution iterative approach allows the robust segmentation of the entire liver surface without extensive shape prior information and/or significant user interaction to overcome local minima.

Our experimental results show that our algorithm is effective and reliable when compared to the ground-truth and other commercial methods. Our algorithm achieves a more accurate and robust volume estimation than the commercial automatic method when compared to the manual segmentation. Although our segmentation results are not better than those of the commercial interactive tool, our method requires only one pixel seed selection which can be done by a non-expert user in few seconds, while the commercial interactive tool requires more than 5 min of expert user time for the segmentation. Our method can thus be effective for hepatic volume estimation and liver modeling in a clinical setup.

In the future, we plan to extend our method to entire liver analysis, including tumors and vessels segmentation inside the liver, and to apply our algorithm to other medical image segmentation tasks, such as kidney and spleen.

References

1. Okada T, Shimada R, Sato Y, Hori M, Yokota K, Nakamoto M, Chen Y, Nakamura H, Tamura S (2007) Automated segmentation of the liver from 3D CT images using probabilistic Atlas and multi-level statistical shape model. In: Proc of the 10th int conf on medical image computing and computer-assisted intervention (MICCAI'07). Lecture Notes in Computer Science, vol 4791. Springer, Heidelberg, pp 86–93
2. Heimann T, Wolf I, Meinzer HP (2006) Active shape models for a fully automated 3d segmentation of the liver—an evaluation on clinical data. In: Proc of the 9th int conf on medical image computing and computer-assisted intervention (MICCAI'06). Lecture Notes in Computer Science, vol 4191. Springer, Heidelberg, pp 41–48
3. Lamecker H, Lange T, Seebass M (2002) A statistical shape model for the liver. In: Proc of the 5th int conf on medical image computing and computer-assisted intervention (MICCAI'02). Lecture Notes in Computer Science, vol 2489. Springer, Heidelberg, pp 421–427
4. Pohle R, Toennies K (2001) Segmentation of medical images using adaptive region growing. In: Sonka M, Hanson KM (eds) SPIE medical imaging, vol 4322, pp 1337–1346
5. Nakayama Y, Li Q, Katsuragawa S, Ikeda R, Hiai Y, Awai K, Kusunoki S, Yamashita Y, Okajima H, Inomata Y, Doi K (2006) Automated hepatic volumetry for living related liver transplantation at multisection CT. *Radiology* 240(3):743–748
6. Pan S, Dawant M (2001) Automatic 3D segmentation of the liver from abdominal ct images: a level-set approach. In: Sonka M, Hanson KM (eds) SPIE medical imaging, vol 4322, pp 128–138
7. Schenk A, Prause GPM, Peitgen HO (2000) Efficient semiautomatic segmentation of 3d objects in medical images. In: Proc of the 3rd int conf on medical image computing and computer-assisted intervention (MICCAI'00). Lecture Notes in Computer Science, vol 1935. Springer, Heidelberg, pp 186–195
8. Lambrou T, Linney A, Todd-Pokropek A (2007) Wavelet analysis of the liver from CT datasets. In: Proc of the 21st int conf on computer assisted radiology and surgery (CARS'07). Springer, Heidelberg
9. Sosna J, Berman P, Azraq Y, Libson E (2006) Automated liver segmentation and volume calculation from MDCT using a Bayesian likelihood maximization technique: comparison with manual tracing technique. In: 92nd Scientific assembly and annual meeting of the Radiological Society of North America (RSNA'06)
10. Gao L, Heath DG, Kuszyk BS, Fishman EK (1996) Automatic liver segmentation technique for three-dimensional visualization of CT data. *Radiology* 201(2):359–364
11. Soler L, Delingette L, Malandain V, Montagnat J, Ayache N, Koehl C, Dourthe O, Malassagne B, Smith M, Mutter D, Marescaux J (2001) Fully automatic anatomical, pathological, and functional segmentation from CT scans for hepatic surgery. *Comput Aided Surg* 6(3):131–142
12. Chen T, Metaxas D (2005) A hybrid framework for 3d medical image segmentation. *Med Image Anal* 9(6):547–565
13. Teo P, Sapiro G, Wandell B (1997) Anisotropic smoothing of posterior probabilities. In: Proc of the 1997 int conf on image processing (ICIP'97)(3), pp 675–678
14. Perona P, Malik J (1990) Scale-space and edge detection using anisotropic diffusion. *IEEE Trans Patt Anal Mach Intell* 12(7):629–639
15. Caselles V, Kimmel R, Sapiro G (1997) Geodesic active contours. *Int J Comp Vis* 22(1):61–97
16. Ibanez L, Schroeder W, Ng L, Cates J (2005) The ITK software guide, 2nd edn. Kitware, Inc., Clifton Park. <http://www.itk.org/ItkSoftwareGuide.pdf>
17. Melonakos J, Krishnan K, Tannenbaum A (2006) An ITK filter for Bayesian segmentation: *itkbayesianclassifierimagefilter*. *Insight J*
18. Ginneken B.V, Heimann T, Styner, M (2007) 3D Segmentation in the clinic: a grand challenge. <http://www.sliver07.org>